

# **Impacts of diffusion MRI spatial resolution on the short-range association fiber reconstruction and connectivity estimation**

Jialan Zheng<sup>1,2</sup>, Cong Yang<sup>3</sup>, Wen Zhong<sup>1</sup>, Ziang Wang<sup>4</sup>, Haoxiang Li<sup>1</sup>, Zihan Li<sup>1</sup>, Mingxuan Liu<sup>1</sup>,  
Hongjia Yang<sup>1</sup>, Xiaozhi Cao<sup>5</sup>, Congyu Liao<sup>5</sup>, David H. Salat<sup>6,7</sup>, Susie Huang<sup>6,7</sup>, Qiyuan Tian<sup>1,3</sup>

<sup>1</sup> School of Biomedical Engineering, Tsinghua University, Beijing, China

<sup>2</sup> Tanwei College, Tsinghua University, Beijing, China

<sup>3</sup> Tsinghua Laboratory of Brain and Intelligence, Tsinghua University, Beijing, China

<sup>4</sup> Tsinghua Medicine, Tsinghua University, Beijing, China

<sup>5</sup> Department of Radiology, Stanford University, Stanford, CA, USA

<sup>6</sup> Athinoula A. Martinos Center for Biomedical Imaging, Massachusetts General Hospital, Charlestown, MA, USA

<sup>7</sup> Harvard Medical School, Boston, MA, USA.

**Primary category:** Neuro, Structural Connectivity

**Secondary category:** Diffusion, Tractography

**General keyword:** Brain connectivity

**Other general keyword:** Short-range Association Fibers

## **Synopsis (96 words)**

### **Motivation.**

Short-range association fibers (SAFs) are essential for mediating cortico-cortical communication. However, their accurate mapping requires high-resolution diffusion MRI data since SAFs reside in a ~1.5mm thin layer beneath the cortex.

### **Goal(s).**

Clarify impact of diffusion image resolution on the estimation of SAFs and connectivity.

### **Approach.**

Simulated and empirical diffusion data at different resolutions were obtained for reconstructing structural connectivity matrices. SAF connectivity strength was quantified and compared. The volume fraction and fiber orientation of local SAFs were examined.

### **Results.**

Lower image spatial-resolution leads to disorganized SAF orientation, decreased voxel-wise white matter volume fraction, and underestimation of SAF connectivity strength.

## **Impact (38 words)**

This study demonstrates the poor reconstruction result of SAFs at low resolution, emphasizing the need for high-resolution diffusion imaging for accurately SAF modeling. The gSlider protocol presented in the study could be an ideal choice for SAFs research.

## **Abstract Body (750 words)**

### **Introduction (185 words)**

Short-range association fibers (SAFs), which directly connect adjacent cortical regions (3 to 30 mm), contribute to 90% of all axonal fibers and play a crucial role in mediating cortico-cortical communication and cognitive function<sup>1,2</sup>. However, SAFs reside in a very thin (~1.5 mm) layer of superficial white matter beneath the cortex and their accurate mapping for faithful structural connectome reconstruction requires high spatial resolution to reduce the partial voluming effect with the gray matter and to resolve fiber crossing with long-range fibers that enter the cortex.

Even though connectivity matrices reconstructed from diffusion MRI data at any spatial resolution include short-range connectivity strengths, but their accuracy has never been examined and validated. As advanced high-resolution diffusion MRI methods emerge (e.g., gSlider<sup>3,4</sup>, MB-MUSE<sup>5</sup>) and become more feasible for neuroscientific and clinical applications (e.g., product multi-shot EPI methods MUSE by GE and RESOLVE by Siemens), It is timely to investigate and clarify the impacts of image resolution on SAF reconstruction and connectivity estimation. In this study, we systematically study this crucial question using simulation and empirical diffusion data acquired at different spatial resolutions and widely adopted processing pipelines.

### **Methods (251 words)**

Simulated Data: Simulation used diffusion data of healthy subjects from the Human Connectome Project (HCP)<sup>6</sup>. Pre-processed diffusion data were acquired at 1.25mm isotropic resolution and down-sampled to 1.5, 2, and 2.5mm isotropic resolution, which are commonly used in practice. Co-registered T1w data and FreeSurfer processing results were also used.

Empirical data: With written consent forms and IRB approval, T1w and diffusion data at 0.96, 1.5, and 2 mm isotropic resolution were acquired on 20 healthy subjects on a 3-Tesla scanner (Siemens, MAGNETOM Prisma) equipped with a 32-channel head coil. Imaging protocols are listed in Figure 1<sup>4</sup>. The gSlider sequence was used for acquiring sub-millimeter resolution. gSlider excites the same thick slice 5 times using different RF encodings and computes the thin slices for improved SNR (Figure 1B). Other diffusion data were acquired using the product 2D SMS-PGSE single-shot EPI sequence. B-values and b-vectors for all diffusion data were identical to remove their impacts. The diffusion data were pre-processed using the “topup”<sup>7</sup> and “eddy”<sup>8</sup> function from FSL.

Data analysis (Figure 2): Fiber orientation estimation, probabilistic tractography, and connectivity matrix reconstruction were performed using the widely adopted MRtrix<sup>3</sup><sup>9</sup> and FSL<sup>10</sup> pipeline. Short-range connectivity strength was defined as the ratio between the number of fibers connecting a cortical area and its direct neighbors and the number of all fibers connecting to this cortical area. Fiber orientations from FSL's Ball-and-Stick model<sup>11</sup> in the superficial white matter

were examined. Additionally, volume fraction maps from MRtrix3's constrained spherical deconvolution (CSD)<sup>12</sup> were used to assess partial volume effects.

### **Results ( 220 words)**

Short-range connectivity strength was underestimated at lower spatial resolution (Figure 3). The simulated data showed that as the resolution decreases from 1.25mm to 1.5mm, 2.0mm, and 2.5mm isotropic, the short-range structural connection strength drops from 68.0% to 67.1%, 65.3%, and 63.9% (MRtrix3 pipeline), or from 60.3% to 52.1%, 42.6%, and 37.9% (FSL pipeline). Similarly, for empirical data, at resolutions of 0.96mm, 1.5mm, and 2mm isotropic, the short-range connection strength is 72.4%, 66.8%, and 60.1% (MRtrix3 pipeline), or 60.1%, 53.8%, and 47.1% (FSL pipeline).

Fiber orientation near the cortical surface for SAFs appear inconsistent at lower resolution (Figure 4). Long-range fibers that enter the cortex and SAFs cross near the cortex, which are well-resolved at high resolutions. However, at lower resolutions, the fiber crossings become disorganized, rendering the tracking of SAFs difficult. This disarray reduces the probability to form SAFs by probabilistic tractography, leading to underestimation of short-range structural connectivity strength.

White matter volume fraction is significantly reduced in the superficial white matter at lower resolution (Figure 5). At lower resolution, more gray matter and CSF components mix into superficial white matter voxels where SAFs reside. This partial volume effect might negatively impact fiber orientation mapping, especially if models that cannot account for multiple tissue components are used (e.g., tensor and single-tissue single-shell CSD) , leading to failed reconstruction of SAFs.

### **Discussion and Conclusion (112 words)**

Our study demonstrates that short-range connectivity strength is significantly underestimated at lower resolutions. This effect might be more pronounced if models that cannot account for multiple tissue components and crossing fibers, such as the widely adopted tensor model, are used. Future work will evaluate the underestimation effect for DTI and other commonly adopted models and clarify whether and how it diminishes brain wiring changes and differences between patients and healthy controls.

Our proposed acquisition method, which balances SNR and resolution using the state-of-the-art gSlider, enables high angular resolution multi-shell sub-millimeter diffusion imaging around 30 minutes. This method significantly improves the reconstruction of short association fibers and holds great potential for broader application.

### **Acknowledgement**

This work was supported by the National Natural Science Foundation of China (grant number 82302166), Tsinghua University Dushi Program and Startup fund and the Beijing Natural Science Foundation (Project No. QY24283).

## Reference

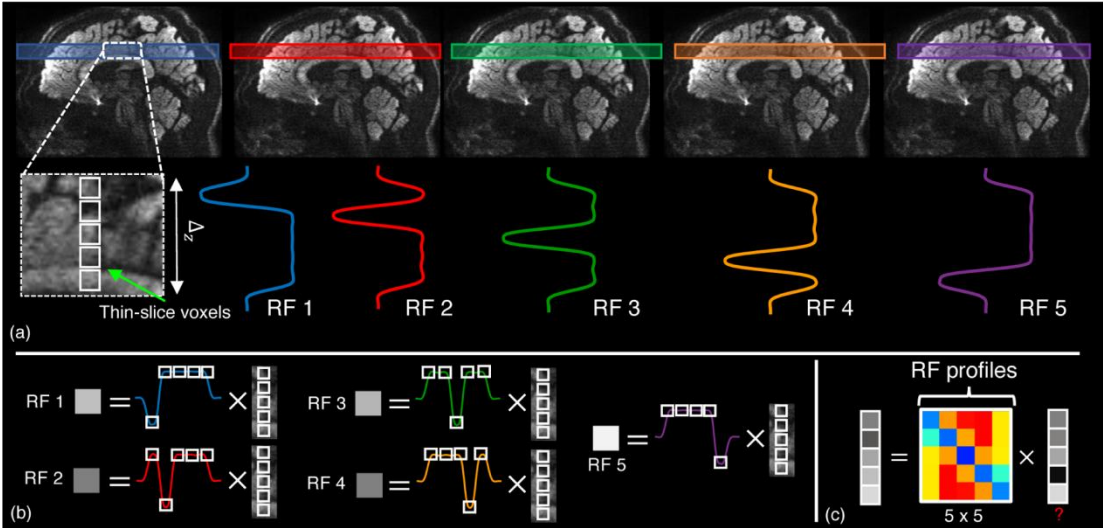
1. Guevara M, Guevara P, Román C, Mangin JF. Superficial white matter: A review on the dMRI analysis methods and applications. *NeuroImage*. 2020;212:116673. doi:10.1016/j.neuroimage.2020.116673
2. Markov NT, Ercsey-Ravasz M, Van Essen DC, Knoblauch K, Toroczkai Z, Kennedy H. Cortical High-Density Counterstream Architectures. *Science*. 2013;342(6158):1238406. doi:10.1126/science.1238406
3. Liao C, Bilgic B, Tian Q, Stockmann JP, Cao X, Fan Q, Iyer SS, Wang F, Ngamsombat C, Lo WC, Manhard MK, Huang SY, Wald LL, Setsompop K. Distortion-free, high-isotropic-resolution diffusion MRI with gSlider BUDA-EPI and multicoil dynamic B0 shimming.
4. Ramos-Llordén G, Ning L, Liao C, Mukhometzianov R, Michailovich O, Setsompop K, Rath Y. High-fidelity, accelerated whole-brain submillimeter in vivo diffusion MRI using gSlider-spherical ridgelets (gSlider-SR). *Magn Reson Med*. 2020;84(4):1781-1795.
5. Ma Y, Bruce IP, Yeh CH, Petrella JR, Song AW, Truong TK. Column-based cortical depth analysis of the diffusion anisotropy and radiality in submillimeter whole-brain diffusion tensor imaging of the human cortical gray matter in vivo. *Neuroimage*. 2023 Apr 15;270:119993.
6. Van Essen DC, Smith SM, Barch DM, Behrens TEJ, Yacoub E, Ugurbil K. The WU-Minn Human Connectome Project: An overview. *NeuroImage*. 2013;80:62-79.
7. Andersson JLR, Skare S, Ashburner J. How to correct susceptibility distortions in spin-echo echo-planar images: Application to diffusion tensor imaging. *NeuroImage*. 2003;20(2):870-888.
8. Andersson JLR, Sotiropoulos SN. An integrated approach to correction for off-resonance effects and subject movement in diffusion MR imaging. *NeuroImage*. 2016;125:1063-1078.
9. Tournier JD, Smith R, Raffelt D, Tabbara R, Dhollander T, Pietsch M, Christiaens D, Jeurissen B, Yeh CH, Connelly A. MRtrix3: A fast, flexible and open software framework for medical image processing and visualisation. *NeuroImage*. 2019;202:116137.
10. Smith SM, Jenkinson M, Woolrich MW, Beckmann CF, Behrens TEJ, Johansen-Berg H, Bannister PR, De Luca M, Drobnjak I, Flitney DE, Niazy RK, Saunders J, Vickers J, Zhang Y, De Stefano N, Brady JM, Matthews PM. Advances in functional and structural MR image analysis and implementation as FSL. *NeuroImage*. 2004;23 Suppl 1:S208-219.
11. Jbabdi S, Sotiropoulos SN, Savio AM, Graña M, Behrens TEJ. Model-based analysis of multishell diffusion MR data for tractography: How to get over fitting problems. *Magn Reson Med*. 2012;68(6):1846-1855.
12. Jeurissen B, Tournier JD, Dhollander T, Connelly A, Sijbers J. Multi-tissue constrained spherical deconvolution for improved analysis of multi-shell diffusion MRI data. *NeuroImage*. 2014;103:411-426.

Figure and Caption

(A) MRI Protocol

	T1w MP-RAGE	gSlider	ep2d_1	ep2d_2
FOV <sub>read</sub> (mm)	256	200	200	200
Slice Thickness (mm)	1	4.8	1.5	2.0
In-Plane Resolution (mm <sup>2</sup> )	1 × 1	0.96 × 0.96	1.5 × 1.5	2.0 × 2.0
TR/TE (ms)	2530 / 2.27	3900 / 80	5400 / 76	5400 / 76
Diffusion Encoding	--	10 × b = 0 32 directions × b = 1000s/mm <sup>2</sup> 64 directions × b = 2500s/mm <sup>2</sup>		
Echo Spacing (ms)	6.8	1.06	0.76	0.76
Acquisition Time (min:sec)	6:03	35:06	10:51	10:33

(B) gSlider Illustration (*Gabriel et al. , MRM 2019*)



**Fig 1. Data acquisition. (A) MRI Protocol.** Protocols are shown for T1w and DWIs acquired under three resolutions. For diffusion encoding, a b0 image was interleaved every 16 DWI acquisitions, and two blip-down b0 images were also acquired. **(B) Schematic of the gSlider Sequence.** The gSlider technique employs five distinct RF waveforms to excite five times thicker slabs, enabling the reconstruction of thin slices from the acquired thick-slab data. This is achieved by resolving the intravoxel signal using the unique RF profiles and applying B0 field corrections for uniformity.

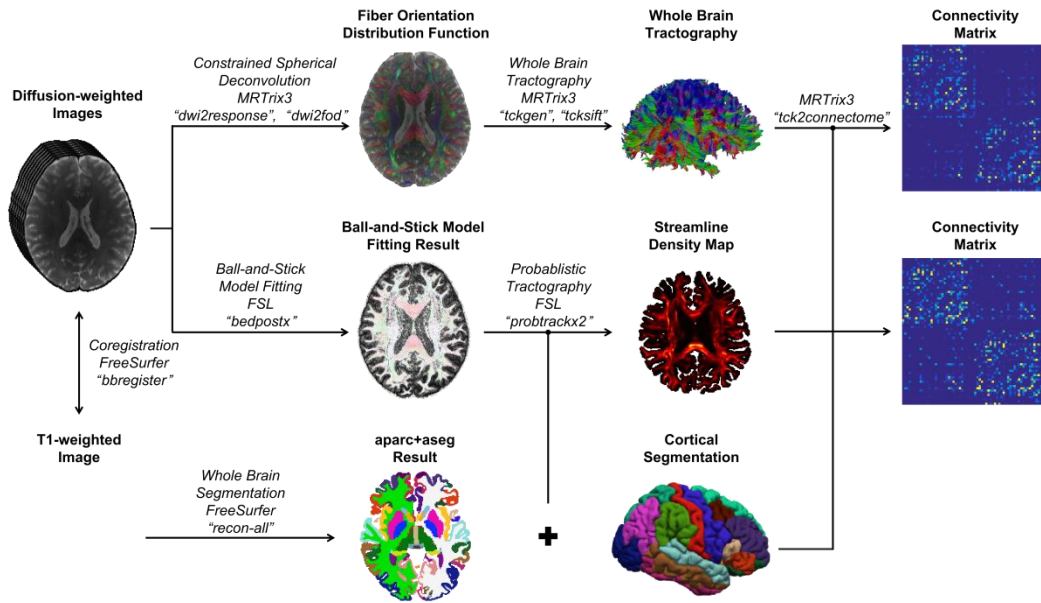


**Fig 2. Data Analysis Pipeline.** Cortical segmentation of T1-weighted image was performed with FreeSurfer, followed by co-registration with diffusion-weighted images. In MRtrix3 pipeline, multi-shell multi-tissue constrained spherical deconvolution was used to derive voxel-wise fiber orientation distribution functions (fODFs) and tissue volume fractions. The fODFs were used to conduct whole-brain tractography and structural connectivity reconstruction. For FSL pipeline, probabilistic tractography was executed following voxel-wise ball-and-stick model estimation.

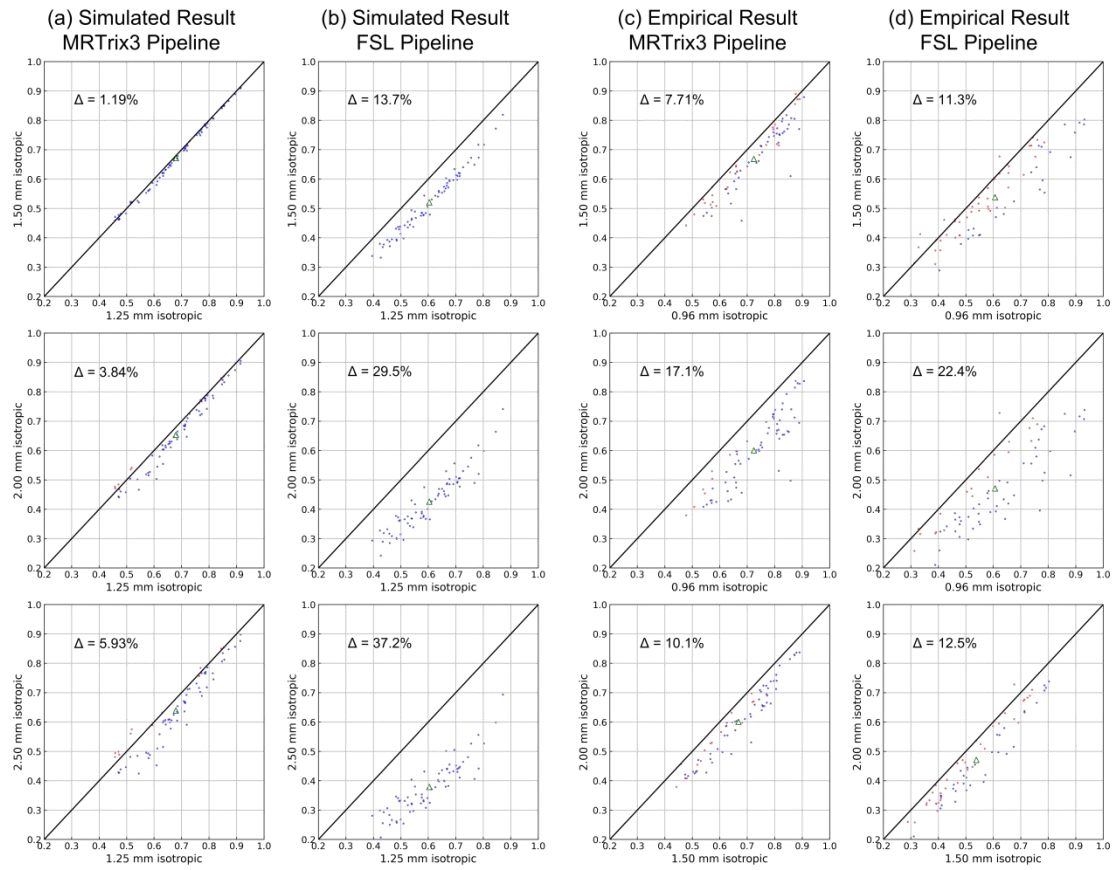


**Fig 3. Short-Range Connection Strength Statistics.** (a), (b) present simulated short-range structural connectivity for all 68 cortices, comparing different resolutions. Paired t-tests are used to evaluate differences in connection strength. Blue dots indicate significantly greater strength at higher resolution at the cortex level, while red dots indicate no such significance. The resolution level values averaged across all cortices are represented by green triangles, all showing significance, with relative differences annotated in upper left. (c), (d) display similar results based on empirical data.

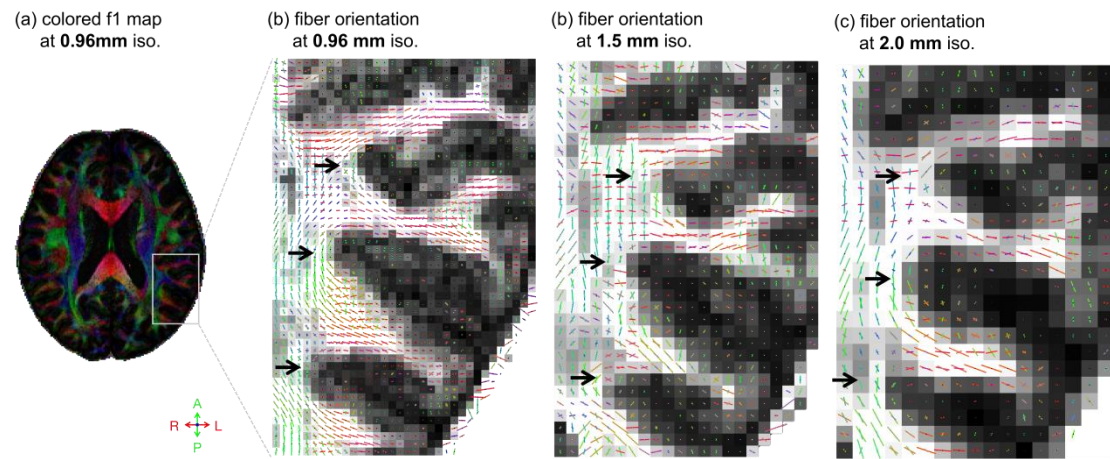


**Fig 4.** Primary and secondary fiber orientations and volume fractions of primary fibers at various resolutions. Arrows indicate the location of short-range fibers. At sub-millimeter resolution, short-range fibers are clearly depicted with smooth distribution (a). At lower resolutions, the partial volume effects result in mixed intravoxel fiber orientations (b, c), thereby interfering the reconstruction of short-range fibers and potentially leading to an underestimation of short-range connectivity.



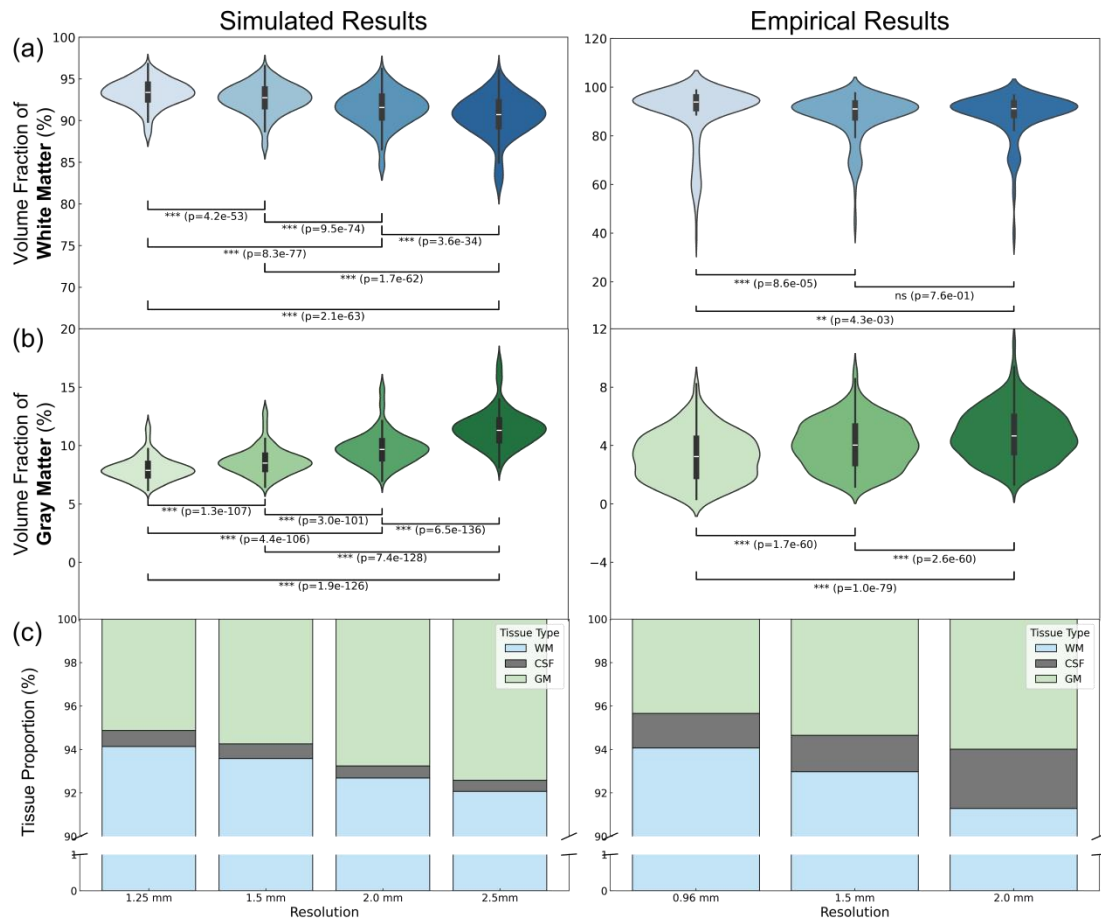


**Fig 5. Volume Fraction Analysis in Short-Range Fibers.** For short-range fibers that connect two neighboring cortices, fiber volume fractions from all voxels they passes are sampled and averaged across subjects. Violin plots show the volume fraction of white (a) and gray (b) matter, including box plots and kernel density estimation. Paired t-tests with Bonferroni correction were used for pairwise comparisons. Panel (c) shows the average tissue composition. The figure indicates a significant decrease of white matter volume fraction and increased partial volume effects at lower resolution.